

# Detection of gamma-ray burst Amati relation based on Hubble data set and Pantheon+ samples

Yufen Han<sup>1</sup>, Jiaze Gao<sup>1</sup>, Gang Liu<sup>1</sup>, Lixin Xu<sup>a,1</sup>

<sup>1</sup>Institute of Theoretical Physics, School of Physics, Dalian University of Technology, Dalian 116024, People's Republic of China

Received: date / Accepted: date

**Abstract** gamma-ray bursts as standard candles for cosmological parameter constraints rely on their empirical luminosity relations and low-redshift calibration. In this paper, we examine the Amati relation and its potential corrections based on the A118 sample of higher-quality gamma-ray bursts, using both Hubble data set and Pantheon+ samples as calibration samples in the redshift range of  $z < 1.965$ . In calibrating gamma-ray bursts using these two datasets, we employ Gaussian processes to obtain corresponding Hubble diagrams to avoid the dependence on cosmological models in the calibration process. We first divided the low-redshift sample of GRBs into two bins and examined the Amati relation and its potential modifications. We found that under both calibrations, the Amati relation did not show evidence of redshift evolution (68% confidence level). For the other two Amati relations that include redshift evolution terms, the central values of the redshift evolution coefficients deviated from 0, but due to the limitations of the sample size and the increase in the number of parameters, most of the redshift evolution coefficients were not able to be excluded from 0 at the  $1\sigma$  level. Therefore, to assess their situation across the entire redshift range, we employed MCMC to globally fit three types of Amati relations. By computing AIC and BIC, we found that for the GRB A118 sample, the standard Amati relation remains the most fitting empirical luminosity formula, and no potential redshift evolution trend was observed for two different low-redshift calibrating sources.

## 1 Introduction

In 1998, two independent research groups measured the relation between the distance and redshift of type Ia supernovae to accurately determine the matter density within the range of  $0 < z < 0.7$ , which showed that the universe was in an

accelerating expansion phase [1, 2]. Since then, other observations such as cosmic microwave background radiation (CMB) [3–6] and baryon acoustic oscillations (BAO) [7, 8] have confirmed that the universe is in an accelerating expansion. The accelerated expansion of the universe implies that the current cosmic evolution is predominantly governed by a substance with negative pressure, known as dark energy. However, our understanding of the dark energy component dominating the current universe evolution remains incomplete to date, necessitating the exploration of cosmological probes at higher redshifts.

The mechanism of standard type Ia supernovae (SNe Ia) limits their maximum luminosity, with observed redshifts typically around  $z \sim 2.3$  [9], which can be used as a probe for studying cosmology [10–14]. Clearly, to extend cosmological studies to higher redshifts, gamma-ray bursts (GRBs) can serve as complementary cosmic probes. The maximum redshift of gamma-ray bursts observed so far can reach approximately  $z \sim 9.4$  [15], with luminosities ranging from  $10^{47}$  erg s<sup>-1</sup> to  $10^{54}$  erg s<sup>-1</sup> [16].

When utilizing gamma-ray bursts as cosmological supplementary probes, this is based on some empirical luminosity correlations for their standardization [17–29]. Additionally, Amati et al. [30] utilized Hubble observational data to approximate the Hubble function through a linear combination of Bernstein basis polynomials, obtaining Bzier parameter curves. They employed Observable Hubble Data (OHD) to construct luminosity distance in a model-independent manner. Ghirlanda et al. [31] employed gamma-ray bursts with a narrow range of redshifts to calibrate the  $E_p - E_\gamma$  (gamma-ray energy corrected for beaming) relation. Xu [32] utilized a model-independent method to calibrate GRBs, primarily employing internally calibrated gamma-ray bursts for measurements.

However, during the calibration of gamma-ray bursts, ensuring their standardizability is crucial, as noted in Ref. [33].

<sup>a</sup>e-mail: lxxu@dlut.edu.cn (corresponding author)

When employing empirical luminosity relations for GRB calibration, some analyses rely on cosmological models, thereby biasing constraints on cosmological parameters towards assumed cosmological models. Khadka and Ratra [33] analyzed GRB data across six different cosmological models and revealed that the Amati relation remains independent of cosmological models. This indicates that this sample of GRBs can be calibrated using the Amati relation, thereby enabling its application in cosmological studies.

When using calibrated gamma-ray bursts for cosmological studies, overcoming the so-called circularity problem is essential. One approach is simultaneous fitting, where GRBs are jointly fitted with other cosmological phenomena. This approach entails the simultaneous fitting of relevant parameters within GRBs and parameters of the cosmological model [33–45]. Additionally, the distance ladder approach can be employed. When employing the distance ladder approach to calibrate GRBs, it is crucial to select an appropriate standard probe. This assumes that the chosen probe maintains a standardized absolute value consistently from the proximal to the distal ends of the cosmic distance ladder. In accordance with Dainotti et al. [25, 46, 47], it is considered that gamma-ray bursts exhibit a luminosity distance-redshift relation consistent with that of type Ia supernovae at low redshifts, and this relation is subsequently extended to the high-redshift regime of GRBs.

Calibrating gamma-ray bursts (GRBs) using the distance ladder concept, the correlation coefficient of GRBs low redshift empirical luminosity relation is obtained. If it is directly extended to high redshift, it is ignored that the correlation coefficient of empirical luminosity relation may evolve with redshift. For example, Lin et al. [48] found possible redshift evolution in several correlations (including  $E_p - E_{\gamma,iso}$  correlation), but no significant redshift evolution was found in the  $E_p - E_\gamma$  relation. Furthermore, Xu et al. [49] expanded the Dainotti relation by incorporating a redshift evolution term. By assessing the coefficient of this term, they investigated whether this relation evolves with redshift. Then, following the approach outlined in Ref. [50], they employed the Efron-Petrosian method [51] to remove potential evolution in this parameter.

When calibrating the gamma-ray burst Amati relation with a low-redshift probe, taking into account that the obtained correlation coefficients at low redshift may evolve with redshift, Wang et al. [52] and Demianski et al. [53] extended the Amati relation differently by adding a redshift evolution term to describe the redshift evolution of the photometric empirical relation by calibrating the Amati relation with the GRBs. The obtained correlation coefficients at low redshifts were expanded to high redshifts to obtain the distance modulus at high redshifts of the gamma-ray bursts, and the calibrated gamma-ray bursts were used to constrain the cosmological parameters. In this paper, we will also calibrate

gamma-ray bursts based on the concept of the distance ladder, assess the redshift evolution of the Amati relation, and explore the Amati relation and its potential modifications across different redshift bins. Additionally, we will discuss and analyze which of these three empirical luminosity relations better fits the data points.

In this paper, we reconstructed the relation between redshift  $z$  and distance modulus  $\mu$  using Gaussian processes based on the Hubble dataset and the SNe Ia Pantheon+ samples, obtaining the values and errors of the distance modulus for GRBs in the redshift range from 0.0331 to 1.965. We performed binning on low-redshift data of gamma-ray bursts and obtained the correlation coefficients of the Amati relation and its extended version for different bins using MCMC sampling. We then assessed the fitting results of the three relations to the data. We further performed a global fit of the Amati relation and its extended version using MCMC sampling. By calculating AIC and BIC, we selected the empirical luminosity relation that provides a better fit to the data. We then extended the correlation coefficients to higher redshifts, obtaining the distance modulus corresponding to the redshifts of high-redshift gamma-ray bursts. Additionally, we extended the Hubble diagram to higher redshifts.

The structure of this paper is as follows. In Section 2, we reconstruct the relation between redshift and distance modulus of two kinds of data, namely Hubble dataset  $H(z)$  and Pantheon+ samples, respectively by Gaussian process, and obtain the distance modulus of low redshift corresponding to GRBs. In Section 3, we calibrate the Amati relation of gamma-ray bursts and its potential modifications. We calculate, analyze, and discuss these three relations separately. By selecting the appropriate relation and applying its corresponding coefficients, we obtain the distance modulus for high-redshift gamma-ray bursts. This allows us to extend the Hubble diagram to higher redshifts. Section 4 summarizes and discusses the obtained results.

## 2 Data selection and reconstruction of the relation between low redshift and distance modulus

### 2.1 GRBs

In this paper, we selected the A118 sample from Ref. [39] for our gamma-ray burst dataset because it has been demonstrated therein to be standardized, possessing higher quality, and more suitable for cosmological research [39, 54]. This sample comprises 118 long GRB data points with redshifts ranging from 0.3399 to 8.2000. Notably, it has been noted that there is an error in the  $E_p$  value for the GRB081121 data point [29, 43]. Therefore, in this paper, we utilize the corrected value as provided in Ref. [55].

Due to the use of low-redshift calibrated astrophysical objects, with a maximum observed redshift of 1.965, we

can reconstruct the corresponding distance modulus for each redshift based on cosmological principles. Consequently, we can also derive the distance modulus values for gamma-ray burst data points with redshifts lower than 1.965, comprising a total of 48 data points. At the same time, in order to determine whether the empirical luminosity relation of gamma-ray bursts evolves with redshift at low redshifts and to explore the differences among these relations at different redshift ranges, we divided these 48 GRB samples into two parts. The low-redshift subset consists of 24 data points, with a redshift range of  $0.3399 < z < 1.46$ , while the high-redshift subset comprises 24 data points, with a redshift range of  $1.48 < z < 1.95$ .

## 2.2 $H(z)$

The Hubble parameter characterizes the relative expansion rate of the universe and encapsulates valuable information regarding the cosmic expansion history, rendering it a crucial cosmological observable. In this paper, we utilized the updated Hubble parameter data from Table I in reference [45] to calibrate gamma-ray bursts. The dataset comprises 32 data points within a redshift range of  $0.07 < z < 1.965$ , providing values for  $z$ ,  $H(z)$ , and  $\sigma_{H(z)}$ . Notably, 15 of these measurements are correlated. In subsequent analyses, we employed the complete covariance matrix.

In a spatially flat universe, the formula for luminosity distance is as follows:

$$d_L = c(1+z) \int_0^z \frac{1}{H(z')} dz'. \quad (1)$$

Here,  $c$  represents the speed of light, and  $z$  denotes redshift, which can be calculated using Hubble data to obtain the luminosity distance corresponding to each redshift value.

## 2.3 SNe Ia

Type Ia supernovae stand as indispensable celestial phenomena within the domain of cosmological investigations, wielding significant influence in our quest to unravel the mysteries of the universe. In this paper, we use the Pantheon+ samples<sup>1</sup> of SNe Ia, which consists of 1701 light curves of 1550 spectroscopically confirmed Ia supernovae from 18 different sky surveys, with redshifts in the range of  $0.00122 < z < 2.26137$  [56, 57].

In a spatially flat universe, the distance modulus of a supernova observation from an observational point of view is:

$$\mu_{SN} = m_B - M, \quad (2)$$

<sup>1</sup><https://github.com/PantheonPlusSH0ES/DataRelease>.

where  $m_B$  is the apparent magnitude,  $M$  is the absolute magnitude. In this paper, we use a Gaussian prior from the Cepheid calibration distance ladder method. As discussed by Efstathiou [58], the SH0ES prior should be applied to  $M$  rather than  $H_0$  when combining SH0ES data with other astrophysical data in order to constrain the late-time physics. We selected the result  $M = -19.253 \pm 0.027$  from Riess et al. [59] calibrating SNe Ia via Cepheid. Since  $M$  is a posterior derived from the Cepheid calibration of the Pantheon+ samples with redshift  $z < 0.01$ , we selected 1590 data points with redshift  $z > 0.01$  for use.

## 2.4 Reconstructing the relation between low redshift and distance modulus via the Gaussian process

In recent years, Gaussian processes have found extensive application in cosmology [60]. Gaussian processes are an extension of Gaussian distributions, where Gaussian distributions describe the random distribution of variables, whereas Gaussian processes aim to construct the distribution function of random variables [61]. In Gaussian process, the joint distribution of any finite random variables is a multivariate Gaussian distribution, and the covariance between different random variables is determined by a kernel function. Specifically, a Gaussian process can be fully described by a mean function and a covariance function. Given any set of input data points, the Gaussian process can generate the corresponding output value, and the prediction of any input data point is accompanied by an estimate of uncertainty. Thus, without assuming a specific parametric form, Gaussian processes can reconstruct the function from data points via a point-to-point Gaussian distribution [61].

In this paper, we use GaPP<sup>2</sup> [61] to implement Gaussian processes. GaPP is an open-source Python tool that provides methods for Gaussian process regression, allowing reconstruction of functions and their first, second, and third-order derivatives from observed data. Next, we proceed with a brief introduction to Gaussian processes. Observational data can be described using Gaussian processes, for a Gaussian noise  $\epsilon_i$  with variance  $\sigma_i^2$ , the actual observation  $y_i = f(x_i) + \epsilon_i$ , whose Gaussian process can be written as:

$$y \sim \mathcal{N}(\boldsymbol{\mu}, K(\boldsymbol{X}, \boldsymbol{X}) + C). \quad (3)$$

Here,  $\mathcal{N}$  represents the Gaussian process, the covariance matrix  $K(\boldsymbol{X}, \boldsymbol{X})$  is derived from the kernel function  $k(x_i, x_j)$ ,  $\boldsymbol{\mu}$  denotes the mean of the reconstructed function, and  $C$  represents the covariance matrix of the observational data. If the data points are uncorrelated, then their covariance matrix can be expressed as a simple diagonal matrix.

The kernel function of a Gaussian process is a critical component that determines both the prior and posterior

<sup>2</sup><https://github.com/carlosandrepaes/GaPP>.

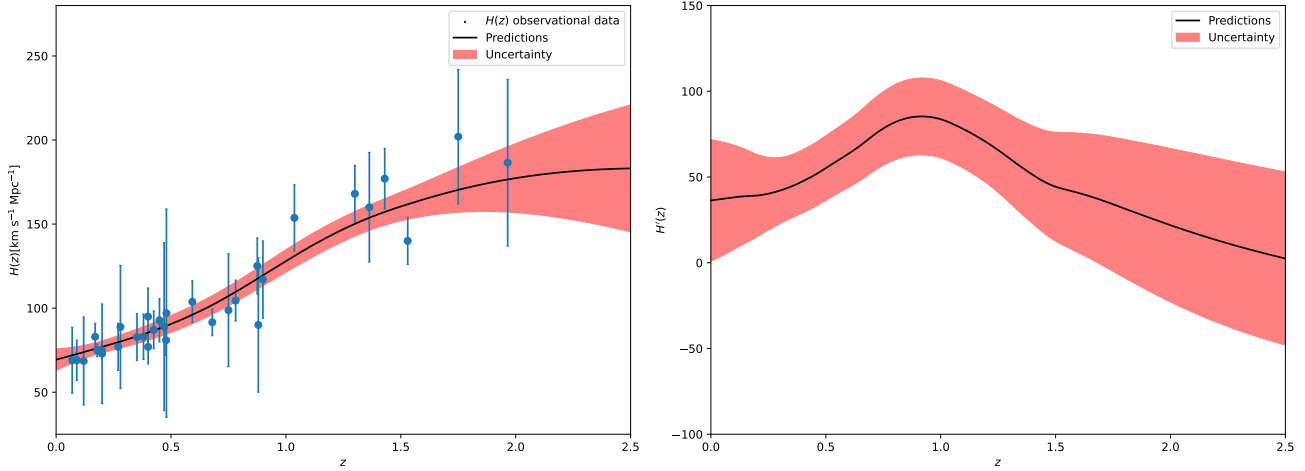


**Fig. 1** The reconstruction of the  $z - H(z)$  plot using GaPP. In the plot, the blue dots represent the data points of the Hubble parameter,  $H(z)$ , along with the associated  $1\sigma$  error bars. The black line represents the reconstructed Hubble data using GaPP, while the shaded red region denotes the  $1\sigma$  error of the reconstructed data.

shapes of the Gaussian process. Each kernel function possesses distinct characteristics and can capture various types of patterns. The covariance function dictates the smoothness and variability of the predictive outcomes. Among the commonly used kernel functions is the squared exponential covariance function [62], expressed as:

$$k(x, \tilde{x}) = \sigma_f^2 \exp\left[-\frac{(x - \tilde{x})^2}{2\ell^2}\right]. \quad (4)$$

Here,  $\sigma_f$  and  $\ell$  are referred to as hyperparameters.  $\sigma_f$  denotes the correlation strength, representing the typical variation of the signal in the  $f(x)$  direction, while  $\ell$  signifies the correlation length, indicating the distance along the  $x$  direction over which significant changes in the function value  $f(x)$  occur. They do not directly determine the form of the correlation function but influence the fluctuations in function values based on the degree of correlation between the data. The optimal hyperparameters are obtained from maximizing the logarithm of the marginalized likelihood function. The logarithmic form of the marginalized likelihood function is expressed as:

$$\ln \mathcal{L} = -\frac{1}{2}(\mathbf{y} - \boldsymbol{\mu})^T [K(\mathbf{X}, \mathbf{X}) + C]^{-1}(\mathbf{y} - \boldsymbol{\mu}) - \frac{1}{2} \ln |K(\mathbf{X}, \mathbf{X}) + C| - \frac{N}{2} \ln 2\pi, \quad (5)$$

where  $N$  is the number of data points.

Next, we proceed with the Gaussian Process reconstruction of the selected low-redshift probes. Initially, we employ GaPP to reconstruct the relationship between redshift  $z$  and Hubble parameter  $H(z)$  using the Hubble dataset. Given the interdependence among certain observations within this dataset, careful handling of both the covariance matrix and observational data is paramount. Specifically, the Hubble

dataset comprises 32 data points, where the first 17 data points exhibit diagonal covariance matrices, while the subsequent 15 data points demonstrate correlated measurements. The correlated covariance matrix can be accessed at <https://gitlab.com/mmoresco/CCcovariance/>. For our analysis, we utilize the complete covariance matrix.

By examining the effect of different kernel functions on the reconstruction of the Hubble dataset, we find that as the differentiability of the kernel increases (large  $\nu$  in the Matrn class), we expect the reconstruction results to be smoother. This is due to stronger correlations and smaller errors or confidence intervals [63]. Ultimately, we chose Matrn ( $\nu = 3/2$ ) for reconstructing  $H(z)$ . This choice not only provides similar mean function results to those obtained with other kernel functions but also ensures that the reconstruction results adhere to the maximum error budget.

The expression for the Matrn ( $\nu = 3/2$ ) covariance function is:

$$k(x, \tilde{x}) = \sigma_f^2 \exp\left[-\frac{\sqrt{3}|x - \tilde{x}|}{\ell}\right] \left(1 + \frac{\sqrt{3}|x - \tilde{x}|}{\ell}\right), \quad (6)$$

The results of Gaussian process reconstruction  $z - H(z)$  are shown in Fig. 1.

Therefore, we can know the value of  $H(z)$  corresponding to each redshift, and the value of photometric distance  $d_L$  corresponding to each redshift  $z$  can be obtained by numerical integration calculation through Eq. (1), and according to the error transfer formula, we can get the error value of photometric distance with the expression:

$$\sigma_{d_L}^2 = \left\{ \left[ c \int_0^z \frac{1}{H(z')} dz' + c(1+z) \frac{1}{H(z)} \right] \sigma_{H(z)} \left( \frac{\partial H(z)}{\partial z} \right)^{-1} \right\}^2 \Big|_{z=z_i}. \quad (7)$$

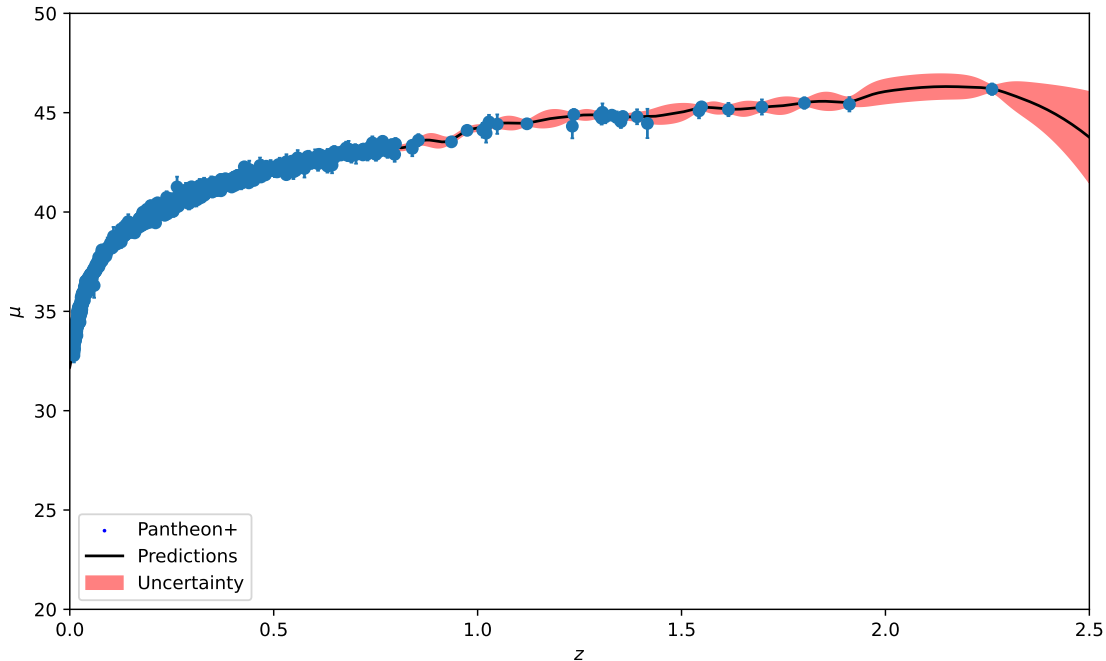


**Fig. 2** GaPP reconstructed  $z - \mu$  plots, where the blue dots are the SNe Ia Pantheon+ data points and  $1\sigma$  errors, the black line is the GaPP reconstructed type Ia supernovae data, and the red region is partly the  $1\sigma$  errors of the reconstructed data.

Moresco et al. [64] analyzed OHD through simulations within the redshift range  $0 < z < 1.5$ , Montiel et al. [65] calibrated the Amati relation with OHD for  $z < 1.43$ , Li et al. [66] set a redshift cutoff at  $z = 1.4$  when calibrating GRBs with the Hubble parameter. They considered the Amati relation to be correct, using this empirical luminosity relation to constrain cosmological parameters. In contrast, the purpose of this paper is to detect the Amati relation and its possible correction in the low redshift range, so we use the entire sample of low redshift (i.e., the Hubble dataset with a redshift  $z < 1.965$ ) to calibrate low redshift gamma-ray bursts. The value of the luminosity distance  $\log(d_L)$  and its error  $\sigma_{\log(d_L)}$  (its redshift range is  $0.0331 < z < 1.95$ ) for 48 data points in the sample of Gamma-Ray Burst A118 sample.

Next, we reconstruct the relation between the redshift  $z$  of type Ia supernovae and the distance modulus  $\mu$  by Gaussian process. Here, we choose the double squared exponential covariance function, to ensure that the reconstructed function does not exhibit weird oscillations [67]. The expression for the covariance function is as follows:

$$k(x, \tilde{x}) = \sigma_{f1}^2 \exp\left[-\frac{(x - \tilde{x})^2}{2\ell_1^2}\right] + \sigma_{f2}^2 \exp\left[-\frac{(x - \tilde{x})^2}{2\ell_2^2}\right]. \quad (8)$$

The Gaussian process reconstruction of  $z - \mu$  results is shown in Fig. 2. Then, we can know the value of the distance modulus  $\mu$  corresponding to each redshift and its error.

For a given cosmological model, the expression of the distance modulus for predicting redshift is:

$$\mu_{th} = 5 \log\left[\frac{d_L(z, \theta)}{\text{Mpc}}\right] + 25. \quad (9)$$

Then the value of  $\log(d_L)$  can be found with the expression:

$$\log(d_L) = (\mu - 25)/5. \quad (10)$$

According to the error transfer, the error is:  $\sigma_{\log(d_L)} = \frac{1}{5}\sigma_\mu$ .

In Refs.[67, 68], it was noted that the reconstruction function exhibits significant uncertainty within the range of  $1.4 < z < 2.3$ , potentially impacting the comprehensive analysis of data comparison. Consequently, redshifts  $z < 1.4$  were utilized to calibrate the empirical luminosity relation of GRBs. To maintain consistency with the maximum redshift of the Hubble dataset, sample points with SNe Ia redshifts less than 1.95 were employed. According to cosmological principles, identical redshifts correspond to identical luminosity distances, allowing us to determine the value of the luminosity distance  $\log(d_L)$  and its error  $\sigma_{\log(d_L)}$  for the 48 data points in the Gamma-Ray Burst A118 sample.



### 3 Selecting the best Amati relation to expand the Hubble diagram of GRBs

The standard Amati relation [19, 36, 69] is based on the empirical luminosity relation between the peak energy of the still frame ( $E_p$ ) and the isotropic energy ( $E_{iso}$ ). Here,  $E_p = E_p^{obs}(1+z)$ , where  $z$  represents the redshift of the GRB, and  $E_p^{obs}$  is a parameter obtained from the detector database. The expression for the isotropic equivalent energy  $E_{iso}$  emitted by the GRB can be defined as follows:

$$E_{iso} = \frac{4\pi d_L^2 S_{bolo}}{1+z}, \quad (11)$$

where,  $d_L$  denotes the luminosity distance, while  $S_{bolo}$  represents the bolometric flux of GRBs.

In the previous discussion, we reconstructed the relation between the Hubble parameter  $H(z)$  and SNe Ia redshift and distance modulus respectively by Gaussian process, and calculated the luminosity distance value and its error of low redshift gamma-ray bursts. Subsequently, we computed the luminosity distance values and their associated uncertainties for low-redshift gamma-ray bursts (GRBs). With reference to Eq. (11), we are able to deduce the corresponding  $E_{iso}$  values for each redshift  $z$ .

When fitting the calibration relation, the Amati relation can be expressed as a linear regression relation:

$$y_i = a + bx_i, \quad (12)$$

where  $x_i$  is a mathematical function that is related to the peak energy  $E_{p,i}$ , while  $y_i$  is a mathematical function that is associated with the radiative flux  $S_{bolo}$  and distance.

$$x_i = \log \frac{E_{p,i}}{300\text{keV}}, \quad (13a)$$

$$y_i = \log \frac{E_{iso}}{\text{erg}} = \log \frac{4\pi d_L^2 S_{bolo,i}}{1+z} + 2 \log d_L. \quad (13b)$$

The likelihood function for gamma-ray bursts is:

$$\mathcal{L} \propto \prod_i^N \frac{1}{\sqrt{2\pi\sigma_{tot,i}^2}} \times \exp\left(-\frac{(y_i - a - bx_i)^2}{2\sigma_{tot,i}^2}\right), \quad (14)$$

where  $\sigma_{tot,i}^2 = \sigma_{ext}^2 + \sigma_{y_i}^2 + b^2\sigma_{x_i}^2$ , based on the principle of error propagation,

$$\sigma_{x,i} = \frac{\sigma_{E_{p,i}}}{\ln 10 E_{p,i}}, \quad (15a)$$

$$\sigma_{y,i} = \frac{\sigma_{S_{bolo,i}}}{\ln 10 S_{bolo,i}}. \quad (15b)$$

One of the extended forms of the Amati relation, proposed by Wang et al. [52], takes into account the significant statistical evolution observed in the empirical luminosity relation. They suggest that the correlation coefficient may

evolve with redshift. To address this issue, inspired by studies on the evolution of fitting parameters in light curves of supernovae observations and the intrinsic luminosity evolution of gamma-ray bursts (GRBs), they introduce two additional redshift-related terms to represent the redshift evolution of the luminosity empirical relation. To avoid the evolution of the correlation coefficient of the Amati relation at high redshifts, two moderate formulas are chosen to extend the Amati relation, with their respective expressions being:

$$a \rightarrow A = a + \frac{\alpha z}{1+z}, b \rightarrow B = b + \frac{\beta z}{1+z}, \quad (16)$$

so, the expanded form of the Amati relation becomes as follows:

$$y_i = \left(a + \frac{\alpha z}{1+z}\right) + \left(b + \frac{\beta z}{1+z}\right)x_i, \quad (17)$$

here,  $x_i$  and  $y_i$  adhere to the expressions outlined in Eq. (13) of the standard Amati relation. The likelihood function remains identical to the standard form. However, the parameters  $a$  and  $b$  in the likelihood function are aligned with Eq. (16).

Another extension of the Amati relation is proposed by Demianski et al. [53], who introduces redshift-evolution terms into the standard Amati relation, assuming  $g_{iso}(z) = (1+z)^{k_{iso}}$  and  $g_p(z) = (1+z)^{k_p}$ . Then, the de-evolved isotropic equivalent energy  $E'_{iso} = \frac{E_{iso}}{g_{iso}(z)}$ , and  $E'_{p,i} = \frac{E_{p,i}}{g_p(z)}$ . The extended Amati relation becomes:

$$y_i = a + bx_i + (k_{iso} - bk_p) \log(1+z). \quad (18)$$

Of course, we can simplify the above equation by introducing a single average coefficient  $c$ , namely:

$$y_i = a + bx_i + c \log(1+z), \quad (19)$$

where  $x_i$  and  $y_i$  also adhere to the expressions outlined in Eq. (13) of the standard Amati relation. However, in this case, the likelihood function for gamma-ray bursts is modified to:

$$\mathcal{L} \propto \prod_i^N \frac{1}{\sqrt{2\pi\sigma_{tot,i}^2}} \times \exp\left(-\frac{(y_i - a - bx_i - c \log(1+z_i))^2}{2\sigma_{tot,i}^2}\right). \quad (20)$$

The  $\sigma_{tot,i}^2$  remains consistent with the expression in the standard Amati relation.

In Section 2, we obtained the distance modulus corresponding to the low redshift of gamma-ray bursts by reconstructing the low-redshift calibration stars through a Gaussian process. Next, we utilize the open-source software package Cobaya [70] as the sampling tool for Markov Chain

Monte Carlo (MCMC) sampling. MCMC is a powerful statistical technique employed for sampling from complex probability distributions. This method utilizes the Metropolis-Hastings algorithm and, aided by a uniform prior probability distribution, generates a chain of sample points to sample from the parameter space.

Firstly, we sampled different bins of gamma-ray bursts with MCMC to obtain Amati and its possible modified correlation coefficients. Then, MCMC was used to globally fit the three relations. The results are shown in Table 1.

Based on Table 1, it is observed that for the standard Amati relation, the constraint results of its free parameters in different bins are consistent within the  $1\sigma$  confidence level, indicating no significant evidence for the redshift evolution of the Amati relation. In contrast, for the two extended Amati relations, the tension between the parameter constraints from low-redshift and high-redshift data is alleviated due to the inclusion of additional parameters to describe redshift dependence, as compared to the standard Amati relation. However, the introduction of extra free parameters may introduce considerable uncertainty. As shown in Table 1, the errors in the coefficients of the two extended Amati relations are larger, which could weaken their constraining power.

Furthermore, through the calibration of the empirical luminosity relations of GRBs with  $H(z)$  and the Pantheon+ samples, the central values of the redshift evolution coefficients in the two extended Amati relations encompass 0 within the  $1\sigma$  range across different bins. Therefore, to further compare these three empirical luminosity relations, a global fitting was performed over the entire redshift range, and the Akaike Information Criterion (AIC) and Bayesian Information Criterion (BIC) were calculated for comparison.

The Akaike Information Criterion (AIC) [71, 72] is a standard for evaluating the complexity of statistical models and measuring the goodness of fit of statistical models. It assesses the relative merits of models by considering the maximum likelihood estimate of the model and the number of parameters in the model. In AIC, penalties for model complexity increase with the number of parameters, thereby avoiding the selection of overly fitted models. In general, it is expressed as:

$$\text{AIC} = 2k - 2 \ln(\mathcal{L}), \quad (21)$$

where  $k$  is the number of fitting parameters, and  $\mathcal{L}$  is the maximum value of the likelihood function. Specifically, the AIC value approaches negative infinity as the goodness of fit tends to its limit, with smaller numerical values representing better ability of the model to explain the data.

The Bayesian Information Criterion (BIC) [73] is another statistical criterion employed for model selection. It assesses models by simultaneously considering their goodness of fit and complexity, thereby facilitating the selection

of the optimal model through the computation of the probability function and the inclusion of a penalty term for the number of parameters in the model. This approach helps guard against overfitting while providing a balanced method for model selection. Analogous to the Akaike Information Criterion (AIC), its expression is:

$$\text{BIC} = k \ln N - 2 \ln(\mathcal{L}), \quad (22)$$

in this equation,  $k$  and  $\mathcal{L}$  correspond to their definitions within the expression for the Akaike Information Criterion (AIC), while  $N$  represents the number of observed data points utilized in the analysis.

We computed the AIC and BIC values for each of these three relations separately. Typically, model comparisons are made based on the differences in AIC (or BIC), denoted as  $\Delta\text{AIC}$  (or  $\Delta\text{BIC}$ ). Table 1 summarizes the  $\Delta\text{AIC}$  and  $\Delta\text{BIC}$  values, representing the differences in AIC and BIC relative to the reference model (the standard Amati relation).

For the values of  $\Delta\text{AIC}$  and  $\Delta\text{BIC}$ , if  $\Delta\text{AIC}(\Delta\text{BIC}) \lesssim 1$ , it indicates that there is little difference between the two models according to statistical model selection criteria. If  $1 \lesssim \Delta\text{AIC}(\Delta\text{BIC}) \lesssim 5$ , the models are not very close, and there may be a preference for the model with smaller  $\Delta\text{AIC}(\Delta\text{BIC})$ . If  $\Delta\text{AIC}(\Delta\text{BIC}) \gtrsim 5$ , the difference between the models is very significant. By computing  $\Delta\text{AIC}$  and  $\Delta\text{BIC}$ , as shown in Table 1, we can observe that the original standard Amati relation is favored over the two extended Amati relations. Therefore, in the subsequent calculations, we will continue to use the standard Amati relation. When calculating the luminosity distance at high redshifts, we will apply the correlation coefficients obtained from the 48 GRB samples along with their associated errors for the Amati relation.

According to Eq. (13b) and the error propagation formula, we obtain:

$$(\log d_L)_i^{data} = \frac{1}{2} \left( a + b \frac{\log E_{p,i}}{300 \text{keV}} - \log \frac{4\pi S_{bolo,i}}{1+z} \right), \quad (23)$$

$$[\sigma(\log d_L)_i^{data}]^2 = \frac{1}{2} \left[ \sigma_{ext}^2 + \sigma_a^2 + \left( \sigma_b \frac{\log E_{p,i}}{300 \text{keV}} \right)^2 + \left( b \frac{\sigma_{E_{p,i}}}{\ln 10 E_{p,i}} \right)^2 + \left( \frac{\sigma_{S_{bolo,i}}}{\ln 10 S_{bolo,i}} \right)^2 \right]. \quad (24)$$

By incorporating the coefficients and uncertainties of the Amati relation obtained via MCMC for 48 GRBs calibrated with two low-redshift calibration objects, we can derive the logarithmic luminosity distances and their errors for 70 data points at high redshifts ( $1.9685 < z < 8.200$ ).

To extend the Hubble diagram of gamma-ray bursts to high redshifts, we calculate the distance modulus at high redshifts based on Eq. (9). According to error propagation, it can be derived that:

$$\sigma_\mu = 5\sigma_{\log d_L}. \quad (25)$$

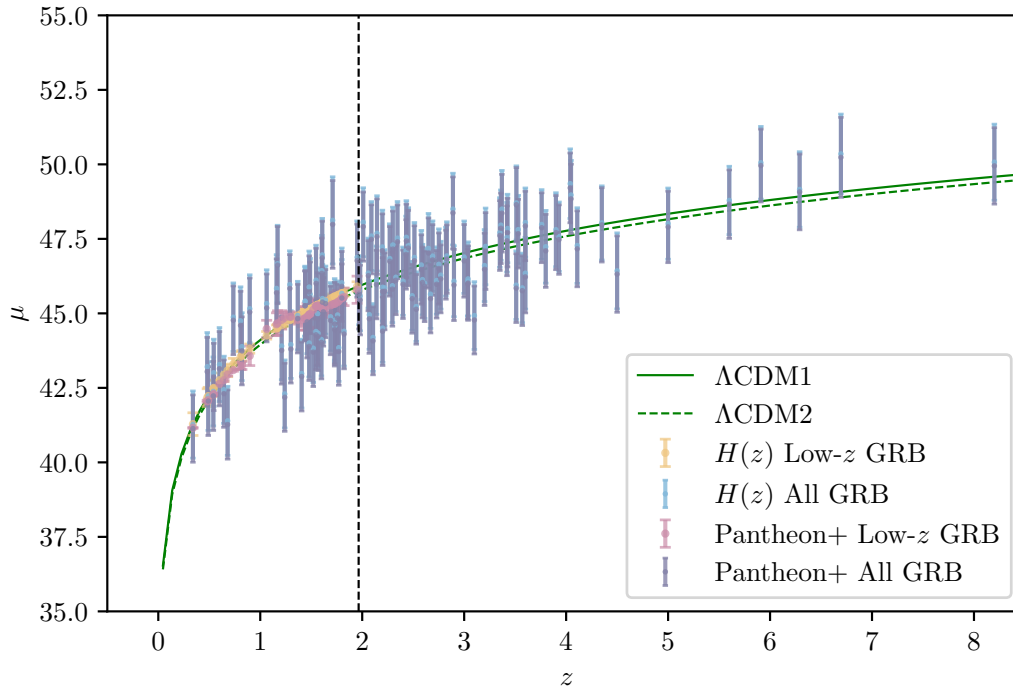


**Fig. 3** Hubble diagram of the A118 sample of gamma-ray bursts, where the yellow dots are the distance moduli of the sample points of the 48 low-redshift gamma-ray bursts obtained from the reconstructed  $H(z)$  data, the blue dots are the distance moduli of the sample of GRBs A118 computed by extending the correlation coefficients of the low-redshift Amati relation obtained by calibrating the  $H(z)$  to high redshifts. The pink dots are the distance moduli of the sample of GRBs A118 obtained from the reconstructed SNe Ia are the distance moduli of the 48 sample points of gamma-ray bursts at low redshift, and the purple dots are the distance moduli of the GRBs A118 sample computed by expanding the correlation coefficients of the low-redshift Amati relation obtained by calibrating the SN to high redshift. The solid green curve is the  $H(z)$  standard distance modulus with  $H_0 = 69.43 \text{ km s}^{-1} \text{ Mpc}^{-1}$ ,  $\Omega_m = 0.309$ . The dashed green curve is the SNe Ia standard distance modulus with  $H_0 = 73.6 \text{ km s}^{-1} \text{ Mpc}^{-1}$ ,  $\Omega_m = 0.334$ . The black dotted line denotes  $z = 1.965$ .

Through calculations, we can determine the distance modulus corresponding to the redshift of the gamma-ray burst sample A118. The Hubble diagram of gamma-ray bursts is illustrated in Fig. 3.

#### 4 Results and discussion

In this paper, based on the concept of the distance ladder, we examine the Amati relation and its possible corrections for the higher-quality gamma-ray burst A118 sample, selecting a more reliable empirical photometric relation, which in turn leads to a model-independent calibration of the gamma-ray bursts, expanding the Hubble diagrams to higher redshift.

We reconstructed the Hubble parameter  $H(z)$  and Pantheon+ samples separately using GaPP, obtaining the distance modulus for each redshift. Based on the principles of cosmology, celestial objects with the same redshift possess the same luminosity distance. Therefore, we were able to derive the corresponding luminosity distances for the 48 low-redshift gamma-ray bursts. Considering that the Amati

relation may evolve with redshift, Wang et al. and Demianski et al. extended this empirical luminosity relation differently. Therefore, we binned the samples at low redshift of GRBs. Through MCMC sampling, we obtained the correlation coefficients for the empirical luminosity relations in different bins. From Table 1, we observe that the correlation coefficients of the Amati relation are consistent within the  $1\sigma$  confidence level across different bins, indicating no significant evidence for redshift evolution of the standard Amati relation (at the 68% confidence level). For the other two extended Amati relations, the redshift evolution coefficients include 0 within the  $1\sigma$  range. Subsequently, to further assess their behavior across the entire redshift range, we performed a global fit for these three relations using MCMC sampling and calculated their respective AIC and BIC. By comparing these values with those of the standard Amati relation, we found that the results of  $\Delta\text{AIC}$  and  $\Delta\text{BIC}$  suggest that, for different low-redshift calibrated gamma-ray bursts A118 sample, the standard Amati relation can already adequately fit the data compared to potential modifications of the Amati relation.



**Table 1** Calibration of the gamma-ray burst (GRB) standard Amati relation, Wangs Amati relation, and Demianski's Amati relation using the Hubble data set and Pantheon+ samples, including correlation coefficients and 68% confidence level errors from MCMC analysis across different bins. It is worth noting that the  $\Delta$  AIC and  $\Delta$  BIC in the table represent the differences in AIC and BIC between the standard Amati relation and the other two Amati relations for GRBs.

	$a$	$b$	$c$	$\alpha$	$\beta$	$\sigma_{ext}$	$\Delta$ AIC	$\Delta$ BIC
Hubble data set								
	24Low-z GRBs	$52.90 \pm 0.13$	$1.10 \pm 0.20$			$0.493^{+0.058}_{-0.092}$		
Amati	24High-z GRBs	$53.03 \pm 0.14$	$1.24 \pm 0.22$			$0.408^{+0.065}_{-0.082}$		
	48All GRBs	$52.970 \pm 0.071$	$1.18 \pm 0.14$			$0.445^{+0.043}_{-0.057}$	-	-
Wang's	24Low-z GRBs	$52.53 \pm 0.54$	$0.8^{+1.0}_{-1.3}$	$0.8 \pm 1.1$	$0.6^{+2.6}_{-1.9}$	$0.505^{+0.063}_{-0.096}$		
Amati	24High-z GRBs	$52.5^{+1.8}_{-1.4}$	$1.1^{+1.4}_{-2.6}$	$0.8^{+2.1}_{-2.9}$	$0.3^{+3.7}_{-2.8}$	$0.407^{+0.055}_{-0.087}$		
	48All GRBs	$52.49 \pm 0.37$	$0.62 \pm 0.93$	$0.88 \pm 0.67$	$0.9 \pm 1.7$	$0.448^{+0.043}_{-0.058}$	13.072482	16.814884
Demianski's								
	24Low-z GRBs	$52.61 \pm 0.37$	$1.06 \pm 0.20$	$1.0 \pm 1.3$		$0.497^{+0.058}_{-0.093}$		
Amati	24High-z GRBs	$52.7^{+1.3}_{-0.79}$	$1.24 \pm 0.22$	$0.8^{+1.7}_{-3.3}$		$0.411^{+0.052}_{-0.089}$		
	48All GRBs	$52.60 \pm 0.28$	$1.12 \pm 0.14$	$1.08 \pm 0.78$		$0.436^{+0.041}_{-0.055}$	3.654998	5.526199
Pantheon+ samples								
	24Low-z GRBs	$52.86 \pm 0.10$	$1.13 \pm 0.20$			$0.499^{+0.061}_{-0.094}$		
Amati	24High-z GRBs	$52.96 \pm 0.13$	$1.27 \pm 0.23$			$0.408^{+0.054}_{-0.087}$		
	48All GRBs	$52.916 \pm 0.071$	$1.20 \pm 0.14$			$0.446^{+0.040}_{-0.054}$	-	-
Wang's	24Low-z GRBs	$52.39 \pm 0.53$	$0.8 \pm 1.2$	$0.99 \pm 1.1$	$0.5 \pm 2.2$	$0.509^{+0.063}_{-0.098}$		
Amati	24High-z GRBs	$52.5^{+2.0}_{-1.2}$	$1.2 \pm 1.8$	$0.7^{+2.1}_{-3.0}$	$0.2 \pm 2.9$	$0.406^{+0.053}_{-0.087}$		
	48All GRBs	$52.42^{+0.33}_{-0.39}$	$0.61 \pm 0.92$	$0.90^{+0.70}_{-0.61}$	$0.9 \pm 1.6$	$0.441^{+0.042}_{-0.056}$	13.12239	16.865792
Demianski's								
	24Low-z GRBs	$52.51 \pm 0.37$	$1.06 \pm 0.21$	$1.3 \pm 1.3$		$0.506^{+0.061}_{-0.094}$		
Amati	24High-z GRBs	$52.6^{+1.2}_{-0.86}$	$1.26 \pm 0.23$	$0.8^{+1.7}_{-3.3}$		$0.407^{+0.054}_{-0.088}$		
	48All GRBs	$552.55 \pm 0.27$	$1.13 \pm 0.15$	$1.05 \pm 0.75$		$0.438^{+0.040}_{-0.057}$	3.873152	5.744353

Therefore, we extend the correlation coefficient of the low redshift of the standard Amati relation directly to the high redshift, and further calculate the distance modulus of the gamma-ray burst at the high redshift, so we extend the Hubble diagram to the higher redshift.

Certainly, due to the limited number of data points and the presence of different empirical luminosity relations for various samples of GRBs, there is considerable controversy regarding whether the correlation coefficients evolve with redshift, as noted in Refs.[74, 75]. Therefore, in order to calibrate gamma-ray bursts as standard candles for cosmological probes, further investigation into whether their empirical luminosity relations evolve with redshift is warranted. We look forward to additional observational data and improved calibration methods to facilitate a more definitive assessment.

**Acknowledgements** This work is supported in part by National Natural Science Foundation of China under Grant No. 12075042 and No. 11675032.

## References

1. A Gladkikh Alexei, L Moore Ron, Jonathan M. Craig, Saurabh Robert, D. Brian, R. Chris, and Brent P. Nicholas. Observational evidence from supernovae for an accelerating universe and a cosmological constant. *arXiv: Astrophysics*, 1998. URL <https://api.semanticscholar.org/CorpusID:230446360>.
2. Saul Perlmutter, Goldhaber Aldering, Gerson Goldhaber, Richard A Knop, Peter Nugent, Patricia G Castro, Susana Deustua, Sebastien Fabbro, Ariel Goobar, Donald E Groom, et al. Measurements of  $\omega$  and  $\lambda$  from 42 high-redshift supernovae. *The Astrophysical Journal*, 517(2):565, 1999.
3. David N Spergel, Licia Verde, Hiranya V Peiris, Eiichiro Komatsu, MR Nolta, Charles L Bennett, Mark Halpern, Gary Hinshaw, Norman Jarosik, Alan Kogut, et al. First-year wilkinson microwave anisotropy probe (wmap)\* observations: determination of cosmological parameters. *The Astrophysical Journal Supplement Series*, 148(1):175, 2003.
4. Planck Collaboration, PAR Ade, N Aghanim, C Armitage-Caplan, M Arnaud, M Ashdown, F Atrio-Barandela, J Aumont, C Baccigalupi, AJ Banday, et al. Planck 2013 results. xvi. cosmological parameters. *A&A*, 571:A16, 2014.
5. Peter AR Ade, Nabila Aghanim, M Arnaud, Mark Ashdown, J Aumont, Carlo Baccigalupi, AJ Banday, RB Barreiro, JG Bartlett, Nicola Bartolo, et al. Planck 2015 results-xiii. cosmological parameters. *Astronomy & Astrophysics*, 594:A13, 2016.
6. Yashar Akrami, M Ashdown, Jonathan Aumont, Carlo Baccigalupi, M Ballardini, Anthony J Banday, RB Barreiro, Nicola Bartolo, S Basak, K Benabed, et al. Planck 2018 results-iv. diffuse component separation. *Astronomy & Astrophysics*, 641:A4, 2020.
7. Daniel J Eisenstein, Idit Zehavi, David W Hogg, Roman Scoccimarro, Michael R Blanton, Robert C Nichol, Ryan Scranton, Hee-Jong Seo, Max Tegmark, Zheng Zheng, et al. Detection of the baryon acoustic peak in the large-scale correlation function of sdss luminous red galaxies. *The Astrophysical Journal*, 633(2):560, 2005.
8. Shadab Alam, Metin Ata, Stephen Bailey, Florian Beutler, Dmitry Bizyaev, Jonathan A Blazek, Adam S Bolton, Joel R Brownstein, Angela Burden, Chia-Hsun Chuang, et al. The clustering of galaxies in the completed sdss-iii baryon oscillation spectroscopic survey: cosmological analysis of the dr12 galaxy sample. *Monthly Notices of the Royal Astronomical Society*, 470(3):2617–2652, 2017.
9. Daniel Moshe Scolnic, DO Jones, A Rest, YC Pan, R Chornock, RJ Foley, ME Huber, R Kessler, Gautham Narayan, AG Riess, et al. The complete light-curve sample of spectroscopically confirmed sne ia from pan-starrs1 and cosmological constraints from the combined pantheon sample. *The Astrophysical Journal*, 859(2): 101, 2018.
10. D. M. Scolnic, D. O. Jones, A. Rest, Y. C. Pan, R. Chornock, R. J. Foley, M. E. Huber, R. Kessler, G. Narayan, A. G. Riess, S. Rodney, E. Berger, D. J. Brout, P. J. Challis, M. Drout, D. Finkbeiner, R. Lunnan, R. P. Kirshner, N. E. Sanders, E. Schlafly, S. Smartt, C. W. Stubbs, J. Tonry, W. M. Wood-Vasey, M. Foley, J. Hand, E. Johnson, W. S. Burgett, K. C. Chambers, P. W. Draper, K. W. Hodapp, N. Kaiser, R. P. Kudritzki, E. A. Magnier, N. Metcalfe, F. Bresolin, E. Gall, R. Kotak, M. McCrum, and K. W. Smith. The complete light-curve sample of spectroscopically confirmed sne ia from pan-starrs1 and cosmological constraints from the combined pantheon sample. *The Astrophysical Journal*, 859(2):101, May 2018. ISSN 1538-4357. doi:10.3847/1538-4357/aab9bb. URL <http://dx.doi.org/10.3847/1538-4357/aab9bb>.
11. Chao Gao, Yun Chen, and Jie Zheng. Investigating the relationship between cosmic curvature and dark energy models with the latest supernova sample. *Research in Astronomy and Astrophysics*, 20(9):151, September 2020. ISSN 1674-4527. doi:10.1088/1674-4527/20/9/151. URL <http://dx.doi.org/10.1088/1674-4527/20/9/151>.
12. Dillon Brout, Dan Scolnic, Brodie Popovic, Adam G. Riess, Anthony Carr, Joe Zuntz, Rick Kessler, Tamara M. Davis, Samuel Hinton, David Jones, W. Darcy Kenworthy, Erik R. Peterson, Khaled Said, Georgie Taylor, Noor Ali, Patrick Armstrong, Pranav Charvu, Arianna Dwomoh, Cole Meldorf, Antonella

- Palmese, Helen Qu, Benjamin M. Rose, Bruno Sanchez, Christopher W. Stubbs, Maria Vincenzi, Charlotte M. Wood, Peter J. Brown, Rebecca Chen, Ken Chambers, David A. Coulter, Mi Dai, Georgios Dimitriadis, Alexei V. Filippenko, Ryan J. Foley, Saurabh W. Jha, Lisa Kelsey, Robert P. Kirshner, Anais Mller, Jessie Muir, Seshadri Nadathur, Yen-Chen Pan, Armin Rest, Cesar Rojas-Bravo, Masao Sako, Matthew R. Siebert, Mat Smith, Benjamin E. Stahl, and Phil Wiseman. The pantheon+ analysis: Cosmological constraints. *The Astrophysical Journal*, 938(2):110, oct 2022. doi:10.3847/1538-4357/ac8e04. URL <https://dx.doi.org/10.3847/1538-4357/ac8e04>.
13. Jiaze Gao, Zhihuan Zhou, Minghui Du, Rui Zou, Jianping Hu, and Lixin Xu. A measurement of hubble constant using cosmographic approach from fast radio bursts and sne ia, 2023. URL <https://arxiv.org/abs/2307.08285>.
  14. Maria Giovanna Dainotti, Giada Bargiacchi, Malgorzata Bogdan, Salvatore Capozziello, and Shigehiro Nagataki. Reduced uncertainties up to 43% on the hubble constant and the matter density with the sne ia with a new statistical analysis, 2024. URL <https://arxiv.org/abs/2303.06974>.
  15. A Cucchiara, Andrew J Levan, Derek B Fox, Nial R Tanvir, TN Ukwatta, Edo Berger, T Krühler, A Küpcü Yoldaş, XF Wu, K Toma, et al. A photometric redshift of  $z = 9.4$  for grb 090429b. *The Astrophysical Journal*, 736(1):7, 2011.
  16. Bing Zhang. Open questions in grb physics. *Comptes Rendus Physique*, 12(3):206–225, 2011.
  17. EE Fenimore, C Cooper, E Ramirez-Ruiz, MC Sumner, A Yoshida, and M Namiki. Gamma-ray bursts and relativistic shells: the surface filling factor. *The Astrophysical Journal*, 512(2):683, 1999.
  18. JP Norris, GF Marani, and JT Bonnell. Connection between energy-dependent lags and peak luminosity in gamma-ray bursts. *The Astrophysical Journal*, 534(1):248, 2000.
  19. L Amati, F Frontera, M Tavani, A Antonelli, E Costa, M Feroci, C Guidorzi, J Heise, N Masetti, E Montanari, et al. Intrinsic spectra and energetics of beposax gamma-ray bursts with known redshifts. *Astronomy & Astrophysics*, 390(1):81–89, 2002.
  20. D.A. Frail. Gamma-ray bursts: jets and energetics. *Nuclear Physics B - Proceedings Supplements*, 132:255–262, 2004. ISSN 0920-5632. doi:<https://doi.org/10.1016/j.nuclphysbps.2004.04.046>. URL <https://www.sciencedirect.com/science/article/pii/S0920563204001033>. Proceedings of the 2nd BeppoSAX Conference: The Restless High-Energy Universe.
  21. Giancarlo Ghirlanda, Gabriele Ghisellini, and Davide Lazzati. The collimation-corrected gamma-ray burst energies correlate with the peak energy of their  $\nu f\nu$  spectrum. *The Astrophysical Journal*, 616(1):331, 2004.
  22. Daisuke Yonetoku, Toshio Murakami, T Nakamura, Ryo Yamazaki, AK Inoue, and K Ioka. Gamma-ray burst formation rate inferred from the spectral peak energy-peak luminosity relation. *The Astrophysical Journal*, 609(2):935, 2004.
  23. Enwei Liang and Bing Zhang. Model-independent multivariable gamma-ray burst luminosity indicator and its possible cosmological implications. *The Astrophysical Journal*, 633(2):611, 2005.
  24. C Firmani, G Ghisellini, Vladimir Avila-Reese, and G Ghirlanda. Discovery of a tight correlation among the prompt emission properties of long gamma-ray bursts. *Monthly Notices of the Royal Astronomical Society*, 370(1):185–197, 2006.
  25. Maria Giovanna Dainotti, Vincenzo Fabrizio Cardone, and Salvatore Capozziello. A time–luminosity correlation for  $\gamma$ -ray bursts in the x-rays. *Monthly Notices of the Royal Astronomical Society: Letters*, 391(1):L79–L83, 2008.
  26. Nan Liang, Wei Ke Xiao, Yuan Liu, and Shuang Nan Zhang. A cosmology-independent calibration of gamma-ray burst luminosity relations and the hubble diagram. *The Astrophysical Journal*, 685(1):354, 2008.
  27. Ryo Tsutsui, Takashi Nakamura, Daisuke Yonetoku, Toshio Murakami, Yoshiki Kodama, and Keitaro Takahashi. Cosmological constraints from calibrated yonetoku and amati relation suggest fundamental plane of gamma-ray bursts. *Journal of Cosmology and Astroparticle Physics*, 2009(08):015, 2009.
  28. M Xu and YF Huang. New three-parameter correlation for gamma-ray bursts with a plateau phase in the afterglow. *Astronomy & Astrophysics*, 538:A134, 2012.
  29. Yang Liu, Fuyong Chen, Nan Liang, Zunli Yuan, Hongwei Yu, and Puxun Wu. The improved amati correlations from gaussian copula. *The Astrophysical Journal*, 931(1):50, 2022.
  30. Lorenzo Amati, Rocco D’Agostino, Orlando Luongo, Marco Muccino, and Maria Tantalò. Addressing the circularity problem in the  $e-p-e$  iso correlation of gamma-ray bursts. *Monthly Notices of the Royal Astronomical Society: Letters*, 486(1):L46–L51, 2019.
  31. Giancarlo Ghirlanda, Gabriele Ghisellini, Lara Nava, Di Brera, Sissa Trieste, and Mpe Garching. Spectral evolution of fermi/gbm short gamma-ray bursts. *Monthly Notices of the Royal Astronomical Society: Letters*, 410, 2010. URL <https://api.semanticscholar.org/CorpusID:10224797>.
  32. Lixin Xu. Cosmological model-independent gamma-ray bursts calibration and its cosmological constraint to

- dark energy. *Journal of Cosmology and Astroparticle Physics*, 2012(04):025, 2012.
33. Narayan Khadka and Bharat Ratra. Constraints on cosmological parameters from gamma-ray burst peak photon energy and bolometric fluence measurements and other data. *Monthly Notices of the Royal Astronomical Society*, 499(1), 9 2020. doi:[10.1093/mnras/staa2779](https://doi.org/10.1093/mnras/staa2779).
  34. Giancarlo Ghirlanda, Gabriele Ghisellini, Davide Lazzati, and Claudio Firmani. Gamma-ray bursts: new rulers to measure the universe. *The Astrophysical Journal*, 613(1):L13, 2004.
  35. Hong Li, JunQing Xia, Jie Liu, GongBo Zhao, ZuHui Fan, and Xinmin Zhang. Overcoming the circular problem for gamma-ray bursts in cosmological global-fitting analysis. *Astrophysical Journal*, 680(1):92–99, 2007.
  36. Lorenzo Amati, Cristiano Guidorzi, Filippo Frontera, Massimo Della Valle, Fabio Finelli, Raffaella Landi, and Enrico Montanari. Measuring the cosmological parameters with the  $e_p$ ,  $i$ – $e$  iso correlation of gamma-ray bursts. *Monthly Notices of the Royal Astronomical Society*, 391(2):577–584, 2008.
  37. Sergey Postnikov, Maria Giovanna Dainotti, Xavier Hernandez, and Salvatore Capozziello. Nonparametric study of the evolution of the cosmological equation of state with sneia, bao, and high-redshift grbs. *The Astrophysical Journal*, 783(2):126, 2014.
  38. Shulei Cao, Joseph Ryan, Narayan Khadka, and Bharat Ratra. Cosmological constraints from higher redshift gamma-ray burst,  $h_1$ /sc $\zeta$  $_{ii}$ /sc $\zeta$  $_{i}$  starburst galaxy, and quasar (and other) data. *Monthly Notices of the Royal Astronomical Society*, 501(1):15201538, December 2020. ISSN 1365-2966. doi:[10.1093/mnras/staa3748](https://doi.org/10.1093/mnras/staa3748). URL <http://dx.doi.org/10.1093/mnras/staa3748>.
  39. Narayan Khadka, Orlando Luongo, Marco Muccino, and Bharat Ratra. Do gamma-ray burst measurements provide a useful test of cosmological models? *Journal of Cosmology and Astroparticle Physics*, 2021(09):042, 2021.
  40. Shulei Cao, Narayan Khadka, and Bharat Ratra. Standardizing dainotti-correlated gamma-ray bursts, and using them with standardized amati-correlated gamma-ray bursts to constrain cosmological model parameters. *Monthly Notices of the Royal Astronomical Society*, 510(2):29282947, December 2021. ISSN 1365-2966. doi:[10.1093/mnras/stab3559](https://doi.org/10.1093/mnras/stab3559). URL <http://dx.doi.org/10.1093/mnras/stab3559>.
  41. Shulei Cao, Maria Dainotti, and Bharat Ratra. Gamma-ray burst data strongly favour the three-parameter fundamental plane (dainotti) correlation over the two-parameter one. *Monthly Notices of the Royal Astronomical Society*, 516(1):1386–1405, 2022.
  42. Shulei Cao, Maria Dainotti, and Bharat Ratra. Standardizing platinum dainotti-correlated gamma-ray bursts, and using them with standardized amati-correlated gamma-ray bursts to constrain cosmological model parameters. *Monthly Notices of the Royal Astronomical Society*, 512(1):439–454, 2022.
  43. Shulei Cao and Bharat Ratra. Using lower-redshift, non-cmb, data to constrain the hubble constant and other cosmological parameters. *Monthly Notices of the Royal Astronomical Society*, April 2022. ISSN 1365-2966. doi:[10.1093/mnras/stac1184](https://doi.org/10.1093/mnras/stac1184). URL <http://dx.doi.org/10.1093/mnras/stac1184>.
  44. MG Dainotti, A L Lenart, A Chraya, G Sarracino, S Nagataki, N Fraija, S Capozziello, and M Bogdan. The gamma-ray bursts fundamental plane correlation as a cosmological tool. *Monthly Notices of the Royal Astronomical Society*, 518(2):2201–2240, 2023.
  45. Shulei Cao and Bharat Ratra. *Physical Review D*, 107(10), May 2023. ISSN 2470-0029. doi:[10.1103/physrevd.107.103521](https://doi.org/10.1103/physrevd.107.103521). URL <http://dx.doi.org/10.1103/PhysRevD.107.103521>.
  46. Maria Giovanna Dainotti, Richard Willingale, Salvatore Capozziello, Vincenzo Fabrizio Cardone, and Micha l Ostrowski. Discovery of a tight correlation for gamma-ray burst afterglows with canonical light curves. *The Astrophysical Journal Letters*, 722(2):L215, 2010.
  47. Maria Giovanna Dainotti, Vincenzo Fabrizio Cardone, Salvatore Capozziello, Michal Ostrowski, and Richard Willingale. Study of possible systematics in the  $l^* x-t^*$  a correlation of gamma-ray bursts. *The Astrophysical Journal*, 730(2):135, 2011.
  48. Hai-Nan Lin, Xin Li, and Zhe Chang. Model-independent distance calibration of high-redshift gamma-ray bursts and constrain on the CDM model. *Monthly Notices of the Royal Astronomical Society*, 455(2):2131–2138, 11 2015. ISSN 0035-8711. doi:[10.1093/mnras/stv2471](https://doi.org/10.1093/mnras/stv2471). URL <https://doi.org/10.1093/mnras/stv2471>.
  49. Fan Xu, Chen-Han Tang, Jin-Jun Geng, Fa-Yin Wang, Yu-Yang Wang, Abudushataer Kuerban, and Yong-Feng Huang. X-ray plateaus in gamma-ray burst afterglows and their application in cosmology. *The Astrophysical Journal*, 920(2):135, oct 2021. doi:[10.3847/1538-4357/ac158a](https://doi.org/10.3847/1538-4357/ac158a). URL <https://dx.doi.org/10.3847/1538-4357/ac158a>.
  50. M. G. Dainotti, A. . Lenart, G. Sarracino, S. Nagataki, S. Capozziello, and N. Fraija. The x-ray fundamental plane of the platinum sample, the kilonovae, and the sne ib/c associated with grbs. *The Astrophysical Journal*, 904(2):97, nov 2020. doi:[10.3847/1538-4357/abbe8a](https://doi.org/10.3847/1538-4357/abbe8a). URL <https://dx.doi.org/10.3847/1538-4357/abbe8a>.
  51. Bradley Efron and Vahé Petrosian. A simple test of independence for truncated data with applications to redshift surveys. *The Astrophysical Journal*, 399:345–352,



1992. URL <https://api.semanticscholar.org/CorpusID:119901387>.
52. Guo-Jian Wang, Hai Yu, Zheng-Xiang Li, Jun-Qing Xia, and Zong-Hong Zhu. Evolutions and calibrations of long gamma-ray-burst luminosity correlations revisited. *The Astrophysical Journal*, 836(1):103, 2017.
  53. M Demianski, E Piedipalumbo, D Sawant, and L Amati. Prospects of high redshift constraints on dark energy models with the  $e_p$  -  $i$  -  $e$  iso correlation in long gamma ray bursts. *Monthly Notices of the Royal Astronomical Society*, 506(1):903–918, 2021.
  54. Shulei Cao and Bharat Ratra. Testing the standardizability of, and deriving cosmological constraints from, a new amati-correlated gamma-ray burst data compilation, 2024. URL <https://arxiv.org/abs/2404.08697>.
  55. J. S. Wang, F. Y. Wang, K. S. Cheng, and Z. G. Dai. Measuring dark energy with the  $E_{iso}$  -  $E_p$  correlation of gamma-ray bursts using model-independent methods. January . doi:10.1051/0004-6361/201526485.
  56. Dan Scolnic, Dillon Brout, Anthony Carr, Adam G. Riess, Tamara M. Davis, Arianna Dwomoh, David O. Jones, Noor Ali, Pranav Charvu, Rebecca Chen, Erik R. Peterson, Brodie Popovic, Benjamin M. Rose, Charlotte M. Wood, Peter J. Brown, Ken Chambers, David A. Coulter, Kyle G. Dettman, Georgios Dimitriadis, Alexei V. Filippenko, Ryan J. Foley, Saurabh W. Jha, Charles D. Kilpatrick, Robert P. Kirshner, Yen-Chen Pan, Armin Rest, Cesar Rojas-Bravo, Matthew R. Siebert, Benjamin E. Stahl, and WeiKang Zheng. The pantheon+ analysis: The full data set and light-curve release. *The Astrophysical Journal*, 938(2), 10 2022. ISSN 0004-637X. doi:10.3847/1538-4357/ac8b7a. URL <https://www.osti.gov/biblio/1893974>.
  57. Dillon Brout, Dan Scolnic, Brodie Popovic, Adam G. Riess, Anthony Carr, Joe Zuntz, Rick Kessler, Tamara M. Davis, Samuel Hinton, David Jones, W. Darcy Kenworthy, Erik R. Peterson, Khaled Said, Georgie Taylor, Noor Ali, Patrick Armstrong, Pranav Charvu, Arianna Dwomoh, Cole Meldorf, Antonella Palmese, Helen Qu, Benjamin M. Rose, Bruno Sanchez, Christopher W. Stubbs, Maria Vincenzi, Charlotte M. Wood, Peter J. Brown, Rebecca Chen, Ken Chambers, David A. Coulter, Mi Dai, Georgios Dimitriadis, Alexei V. Filippenko, Ryan J. Foley, Saurabh W. Jha, Lisa Kelsey, Robert P. Kirshner, Anais Miller, Jessie Muir, Seshadri Nadathur, Yen-Chen Pan, Armin Rest, Cesar Rojas-Bravo, Masao Sako, Matthew R. Siebert, Mat Smith, Benjamin E. Stahl, and Phil Wiseman. The pantheon+ analysis: Cosmological constraints. *The Astrophysical Journal*, 938(2):110, oct 2022. doi:10.3847/1538-4357/ac8e04. URL <https://dx.doi.org/10.3847/1538-4357/ac8e04>.
  58. George Efstathiou. To  $H_0$  or not to  $H_0$ ? *Monthly Notices of the Royal Astronomical Society*, 505(3):3866–3872, 06 2021. ISSN 0035-8711. doi:10.1093/mnras/stab1588. URL <https://doi.org/10.1093/mnras/stab1588>.
  59. Adam G. Riess, Wenlong Yuan, Lucas M. Macri, Dan Scolnic, Dillon Brout, Stefano Casertano, David O. Jones, Yukei Murakami, Gagandeep S. Anand, Louise Breuval, Thomas G. Brink, Alexei V. Filippenko, Samantha Hoffmann, Saurabh W. Jha, W. Darcy Kenworthy, John Mackenty, Benjamin E. Stahl, and WeiKang Zheng. A comprehensive measurement of the local value of the hubble constant with 1 km s<sup>-1</sup> mpc<sup>-1</sup> uncertainty from the hubble space telescope and the sh0es team. *The Astrophysical Journal Letters*, 934(1):L7, jul 2022. doi:10.3847/2041-8213/ac5c5b. URL <https://dx.doi.org/10.3847/2041-8213/ac5c5b>.
  60. Arman Shafieloo, Alex G Kim, and Eric V Linder. Gaussian process cosmography. *Physical Review D*, 85(12): 123530, 2012.
  61. Marina Seikel, Chris Clarkson, and Mathew Smith. Reconstruction of dark energy and expansion dynamics using gaussian processes. *Journal of Cosmology and Astroparticle Physics*, 2012(06):036, 2012.
  62. Christopher KI Williams and Carl Edward Rasmussen. *Gaussian processes for machine learning*, volume 2. MIT press Cambridge, MA, 2006.
  63. E. Colgin and M. M. Sheikh-Jabbari. Elucidating cosmological model dependence with  $h_0$ , 2021. URL <https://arxiv.org/abs/2101.08565>.
  64. Michele Moresco, Raul Jimenez, Licia Verde, Andrea Cimatti, and Lucia Pozzetti. Setting the stage for cosmic chronometers. ii. impact of stellar population synthesis models systematics and full covariance matrix. *The Astrophysical Journal*, 898(1):82, jul 2020. doi:10.3847/1538-4357/ab9eb0. URL <https://dx.doi.org/10.3847/1538-4357/ab9eb0>.
  65. Ariadna Montiel, J I Cabrera, and Juan Carlos Hidalgo. Improving sampling and calibration of gamma-ray bursts as distance indicators. *Monthly Notices of the Royal Astronomical Society*, 501(3):3515–3526, 12 2020. ISSN 0035-8711. doi:10.1093/mnras/staa3926. URL <https://doi.org/10.1093/mnras/staa3926>.
  66. Zihao Li, Bin Zhang, and Nan Liang. Testing dark energy models with gamma-ray bursts calibrated from the observational  $h(z)$  data through a gaussian process. *Monthly Notices of the Royal Astronomical Society*, 521(3):4406–4413, 2023.
  67. Yuhao Mu, Baorong Chang, and Lixin Xu. Cosmography via gaussian process with gamma ray bursts. *Journal of Cosmology and Astroparticle Physics*, 2023(09):041, 2023.



68. Nan Liang, Zihao Li, Xiaoyao Xie, and Puxun Wu. Calibrating gamma-ray bursts by using a gaussian process with type ia supernovae. *The Astrophysical Journal*, 941(1):84, 2022.
69. Lorenzo Amati. The e p, i–e iso correlation in gamma-ray bursts: updated observational status, re-analysis and main implications. *Monthly Notices of the Royal Astronomical Society*, 372(1):233–245, 2006.
70. Jesus Torrado and Antony Lewis. Cobaya: Code for bayesian analysis of hierarchical physical models. *Journal of Cosmology and Astroparticle Physics*, 2021(05):057, 2021.
71. Hirotugu Akaike. A new look at the statistical model identification. *IEEE transactions on automatic control*, 19(6):716–723, 1974.
72. Hirotugu Akaike. Likelihood of a model and information criteria. *Journal of econometrics*, 16(1):3–14, 1981.
73. Gideon Schwarz. Estimating the dimension of a model. *The annals of statistics*, pages 461–464, 1978.
74. S. Basilakos, S. Nesseris, and L. Perivolaropoulos. Is the cmb shift parameter connected with the growth of cosmological perturbations? *Monthly Notices of the Royal Astronomical Society*, 387(3):1126–1130, 2008. doi:[10.1111/j.1365-2966.2008.13303.x](https://doi.org/10.1111/j.1365-2966.2008.13303.x).
75. Ryo Tsutsui, Takashi Nakamura, Daisuke Yonetoku, Toshio Murakami, Yoshiki Kodama, and Keitaro Takahashi. Cosmological constraints from calibrated yonetoku and amati relation suggest fundamental plane of gamma-ray bursts. *Journal of Cosmology and Astroparticle Physics*, 2009(08):015, aug 2009. doi:[10.1088/1475-7516/2009/08/015](https://doi.org/10.1088/1475-7516/2009/08/015). URL <https://dx.doi.org/10.1088/1475-7516/2009/08/015>.